



**HAL**  
open science

# Chemical Surface Grafting of Pt Nanocatalysts for Reconciling Methanol Tolerance with Methanol Oxidation Reaction Activity

Quentin Lenne, Alice Mattiuzzi, Ivan Jabin, Ludovic Troian-Gautier, Jonathan Hamon, Yann R Leroux, Corinne Lagrost

► **To cite this version:**

Quentin Lenne, Alice Mattiuzzi, Ivan Jabin, Ludovic Troian-Gautier, Jonathan Hamon, et al.. Chemical Surface Grafting of Pt Nanocatalysts for Reconciling Methanol Tolerance with Methanol Oxidation Reaction Activity. *ChemSusChem*, 2023, 10.1002/cssc.202201990 . hal-04016046

**HAL Id: hal-04016046**

**<https://hal.science/hal-04016046>**

Submitted on 6 Nov 2023

**HAL** is a multi-disciplinary open access archive for the deposit and dissemination of scientific research documents, whether they are published or not. The documents may come from teaching and research institutions in France or abroad, or from public or private research centers.

L'archive ouverte pluridisciplinaire **HAL**, est destinée au dépôt et à la diffusion de documents scientifiques de niveau recherche, publiés ou non, émanant des établissements d'enseignement et de recherche français ou étrangers, des laboratoires publics ou privés.

# Chemical Surface Grafting of Pt Nanocatalysts for Reconciling Methanol Tolerance with Methanol Oxidation Activity

Quentin Lenne,<sup>[a]</sup> Alice Mattiuzzi,<sup>[b]</sup> Ivan Jabin,<sup>[c]</sup> Ludovic Troian-Gautier,<sup>[c, d]</sup> Jonathan Hamon,<sup>[e]</sup> Yann R. Leroux,<sup>\*[a]</sup> and Corinne Lagrost<sup>\*[a]</sup>

A conceptual challenge toward more versatile direct methanol fuel cells (DMFCs) is the design of a single material electrocatalyst with high activity and durability for both oxygen reduction reaction (ORR) and methanol oxidation reaction (MOR). This requires to conciliate methanol tolerance not to hinder ORR at the cathode with a good MOR activity at the anode. This is especially incompatible with Pt materials. We tackled this challenge by deriving a supramolecular concept where surface-grafted molecular ligands regulate the Pt-catalyst

reactivity. ORR and MOR activities of newly reported Pt-calix[4]arenes nanocatalysts (Pt<sub>C<sub>62</sub></sub>NPs/C) are compared to commercial benchmark PtNPs/C. Pt<sub>C<sub>62</sub></sub>NPs/C exhibit a remarkable methanol tolerance without losing the MOR reactivity along with outstanding durability and chemical stability. Beyond designing single-catalyst material, operable in DMFC cathodic and anodic compartments, the results highlight a promising strategy for tuning interfacial properties.

## Introduction

Direct methanol fuel cells (DMFCs) are considered as a serious alternative for future portable and mobile power conversion devices.<sup>[1–3]</sup> They usually couple the electrochemical methanol oxidation reaction (MOR) at the anode with the oxygen reduction reaction (ORR) at the cathode. The interest in methanol electro-oxidation is currently boosted by the search of alternative to water oxidation at the anodic side. To date, Pt and its derived alloys show the best catalytic activity for both reactions.<sup>[4–9]</sup> In these Pt-based materials, Pt is almost always identified as the catalytic site, capable to break the O–O bond

but also the C–H bond, thus making it especially appealing for MOR. However, Pt materials could be readily poisoned by intermediates compounds produced during the MOR, notably carbon monoxide (CO). This aspect constitutes a major issue for developing efficient devices. The chemisorption of CO on Pt involves the CO 5σ and 2π\* molecular orbitals. They interact with the empty 5d-orbitals of Pt, resulting in an electron density transfer from 5σ to the metal while backdonation from Pt to the CO 2π\* further stabilizes this interaction.<sup>[10,11]</sup>

Improving the MOR catalytic efficiency usually targets a decrease of CO adsorption through an increase of the electron density around the Pt sites. This is often achieved by filling the empty 5d orbitals via alloy formation with foreign metals (e.g., Sn, Pd, etc.).<sup>[10,11]</sup> This strategy leads to efficient catalysts for MOR while being selective to this reaction, because it cannot be successfully applied to ORR. Indeed, the adsorption of dioxygen on such catalytic materials would then be too weak for the O<sub>2</sub> dissociation reaction. On the other hand, Pt–Ru, which is known as a well-performing MOR catalyst, has been reported to favor easier chemisorption of oxygen from water rather than a significant electron transfer around the Pt sites in the Pt–Ru alloys.<sup>[12]</sup> Importantly, nor has Pt–Ru demonstrated any good performance for ORR while being economically less attractive than Pt itself. Actually, it is difficult to find a catalytic single material capable of promoting both ORR and MOR, without deactivation of the ORR activity in the presence of methanol. It is worth outlining that many papers have described materials having both good ORR and MOR activities, for instance<sup>[13–20]</sup> to quote a few. But none of these have demonstrated methanol tolerance during the ORR process, by really performing ORR study in the presence of methanol. To the best of our knowledge, only one paper reports a Pt–Ag/C catalyst that presents catalytic activity for MOR and ORR in the presence of methanol.<sup>[21]</sup> Unfortunately, this material exhibited higher

[a] Dr. Q. Lenne, Dr. Y. R. Leroux, Dr. C. Lagrost  
ISCR-UMR 6226  
Univ Rennes  
Campus de Beaulieu, 35000 Rennes (France)  
E-mail: yann.Leroux@univ-rennes1.fr  
corinne.lagrost@univ-rennes1.fr

[b] Dr. A. Mattiuzzi  
X4C  
48 Auguste Piccard, 6041 Gosselies (Belgium)

[c] Prof. I. Jabin, Dr. L. Troian-Gautier  
Laboratoire de Chimie Organique  
Université libre de Bruxelles  
CP 160/06, avenue F.D. Roosevelt 50, 1050 Brussels (Belgium)

[d] Dr. L. Troian-Gautier  
Institut de la Matière Condensée et des Nanosciences  
Université catholique de Louvain  
Place Louis Pasteur 1, 1348 Louvain-la-Neuve (Belgium)

[e] J. Hamon  
Institut des Matériaux de Nantes\_UMR 6502  
Université de Nantes  
2 rue de la Houssinière, 44000 Nantes (France)

Supporting information for this article is available on the WWW under <https://doi.org/10.1002/cssc.202201990>

© 2023 The Authors. ChemSusChem published by Wiley-VCH GmbH. This is an open access article under the terms of the Creative Commons Attribution License, which permits use, distribution and reproduction in any medium, provided the original work is properly cited.

electrocatalytic properties and stability as anode in alkaline media while having better methanol tolerance as cathode in acidic electrolyte.<sup>[21]</sup>

Herein, we describe a rare example of a catalyst which brings together ORR and MOR electrocatalytic properties combined to cathodic methanol tolerance within a single material. Rather than shaping and/or alloying the platinum surface, organic capping ligands are employed to design such a versatile system. Far to have an adverse impact on catalytic activity, the deliberate surface modification of catalyst has been recently recognized as a powerful approach to design efficient and durable electrocatalysts.<sup>[22,23]</sup> One of the main interest of this approach is that the internal structure, including morphology and strain of metal nanoparticles, remains unchanged in contrast to alloying. However, the concurrent electronic and steric effects due to chemisorbed ligands are generally difficult to regulate. For this, the ligands bonding to the surface and spatial distribution of the chemical functions are important parameters to master. We have recently reported the excellent catalytic properties towards ORR in alkaline media of gold and silver nanoparticles modified through the reductive grafting of calix[4]arene-tetraacetate-tetradiazonium salts.<sup>[22,24]</sup> It is now established that diazonium chemistry enables the formation of highly robust interface with a strong metal-ligands interaction thanks to the establishment of M–C bonds<sup>[25–27]</sup> The rigid macrocyclic structure of the calix[4]arenes leads to formation of a well-ordered covalently-bound monolayer. A fine spatial control is imposed by the small rim geometry and multiple anchoring points at the large rim ensure high stability.<sup>[28]</sup> In addition, the nature of the chemical terminal groups at the small rim can be tuned to control the interactions with reactants and/or intermediates at the electrolyte/catalyst interfaces.

In this context, we report for the first time the one-pot synthesis of platinum nanoparticles functionalized with calix[4]arenes bearing trifluorobutyl groups (Pt<sub>CF<sub>3</sub></sub> NPs) (Figure 1). Because of the diazonium grafting, strong platinum-ligands interactions are obtained while the trifluorobutyl tail is designed on purposes to enhance local oxygen concentration even in the presence of rather high concentration of methanol (0.5 M). The resulting nanoparticles supported on carbon Pt<sub>CF<sub>3</sub></sub> NPs/C show higher ORR and MOR activities than the classical benchmarking PtNPs/C material and, more importantly, exhibit significantly enhanced methanol tolerance and stability. The

strategy using the diazonium functionalization through a one-pot procedure is significantly much simpler than other strategies reported in the literature to reach high performance in ORR and MOR electrocatalysis by employing the alloying or the shaping of the nanomaterials.

## Results and Discussion

### Synthesis and characterization of Pt<sub>CF<sub>3</sub></sub> NPs

Pt nanoparticles functionalized with calix[4]arene bearing trifluorobutyl tail groups at the small rim are obtained through a facile one-pot synthesis involving the simultaneous reduction of the platinum salt (H<sub>2</sub>PtCl<sub>6</sub>) and the corresponding calix[4]arene tetradiazonium salt (calix[4]CF<sub>3</sub>). Upon addition of NaBH<sub>4</sub> as reducing agent, H<sub>2</sub>PtCl<sub>6</sub> and calix[4]CF<sub>3</sub> are reduced to platinum clusters and calix[4]tetra-aryl radicals, respectively. The aryl radicals are formed upon reduction through the departure of N<sub>2</sub> and are able to chemically graft onto the platinum surface.<sup>[25]</sup> This allows the formation of a robust linkage between the calix[4]arenes molecules and the Pt nanoparticles.<sup>[26,29,30]</sup> In addition, herein, the calix[4]arene tetradiazonium cation is designed to form a monolayer onto the surface, as previously demonstrated, which stands in contrast with what is generally observed with simple aryl diazonium salts.<sup>[27,31]</sup> In a previous work, a similar synthetic strategy using a series of calix[4]arene-tetradiazonium salts has led to the ultrathin coating of small gold nanoparticles (6 nm).<sup>[32]</sup> Figure 2 shows representative HRTEM images of the as-prepared Pt nanoparticles with an average core size equal to 3.4 nm and a rather narrow dispersity. The sizes of the Pt<sub>CF<sub>3</sub></sub> NPs are comparable with the typical dimensions of commercial Pt/C catalysts used as comparative sample in the study (Figure S1). In Figure 2, well-defined lattice fringes can be observed for all samples. The spacing is *c.a.* 0.21 nm, corresponding to (111) or (200) lattice spacing of Pt (Figure S2 in the Supporting Information).<sup>[33]</sup>

The chemical grafting of the Pt nanoparticles surface with the calix[4]arene-trifluorobutyl is confirmed through the XPS (X-ray Photoelectrons Spectroscopy) analyses of a deposit of Pt<sub>CF<sub>3</sub></sub> NPs onto a silicon substrate (Figure 3). The signal of fluorine F 1s at 688.4 ± 0.4 eV is characteristic of organic moieties involving fluorinated groups, notably CF<sub>3</sub> groups. Similarly, the

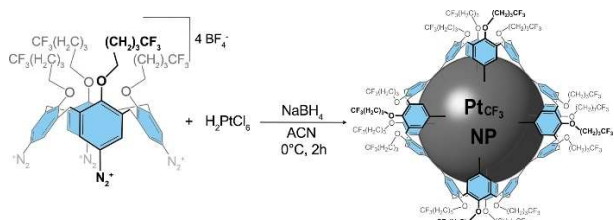


**Figure 1.** Schematic representation of the one-pot synthesis of the platinum nanoparticle functionalized with calix[4]arenes bearing trifluorobutyl groups at the small rim (Pt<sub>CF<sub>3</sub></sub> NPs).

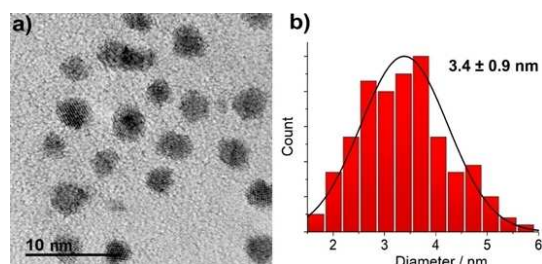


**Figure 2.** a) TEM micrograph and b) the corresponding size distribution of Pt<sub>CF<sub>3</sub></sub> NPs.

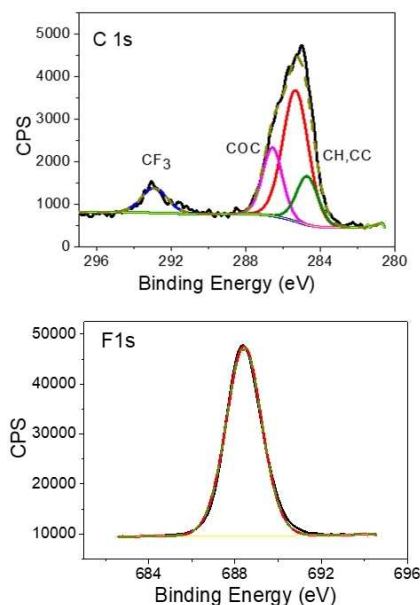


**Figure 3.** High resolution XPS core level spectra of the C 1 s and F 1 s regions of a deposit of Pt<sub>CF<sub>3</sub></sub> NPs onto a silicon substrate.

C 1 s region could be decomposed into components at  $284.8 \pm 0.4$  eV and  $285.3 \pm 0.3$  eV for the carbon atom involved in the aliphatic and aromatic C–H and C–C bonds; at  $286.6 \pm 0.2$  eV for the carbon atoms in the COC bonds and at  $293 \pm 0.2$  eV for the carbon atoms in CF<sub>3</sub> groups. In addition, the atomic ratio between the COC and CF<sub>3</sub> components is equal to 2.09. Such a value fully agrees with the expected theoretical ratio of 2 that takes into account the chemical structure of the calix[4]arene-trifluorobutyl ligands.

### ORR electrocatalytic activity of Pt<sub>CF<sub>3</sub></sub> NPs/C

We first investigate the ORR electrocatalytic activity of Pt<sub>CF<sub>3</sub></sub> NPs to evaluate the influence of the grafted chemical ligands on the catalysts' reactivity toward this reaction. To this purpose, Pt<sub>CF<sub>3</sub></sub> NPs are mixed with carbon (Vulcan XC72) to reach a composition of 20% Pt<sub>CF<sub>3</sub></sub> NPs and 80% carbon. TEM analysis of the supported Pt<sub>CF<sub>3</sub></sub> NPs/C indicates that the nanoparticles are well-dispersed over the carbon surface (Figure S3). By using the same catalyst loading, we could then compare the ORR activity of Pt<sub>CF<sub>3</sub></sub> NPs/C with that of commercially available 20% Pt/C (PtNPs/C), usually considered as benchmark catalyst for ORR in acidic medium. The ORR activity is then studied for the two deposits of carbon-supported nanomaterials onto a GC disk electrode, under the same conditions in O<sub>2</sub>-saturated aqueous 0.1 M HClO<sub>4</sub>. Figure 4 shows the RRDE (Rotating Ring Disk Electrode) voltammetric experiments. The currents are normalized against the Pt mass loading. After iR-drop correction (Figure S5), the ORR onset potentials of PtNPs/C and Pt<sub>CF<sub>3</sub></sub> NPs/C are found equal to 0.83 V and 0.80 V vs. RHE, respectively, while half-wave potentials are determined as 0.71 V and 0.73 V vs. RHE, respectively. Compared to literature data, we thus observe

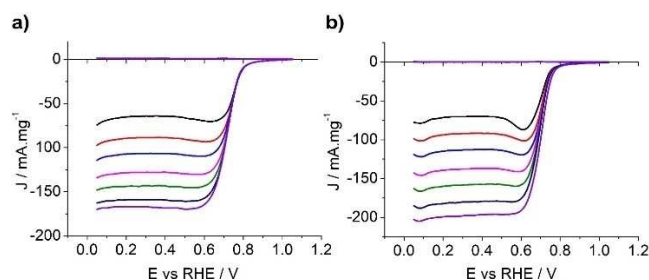
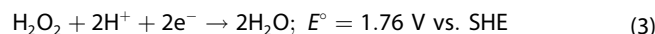
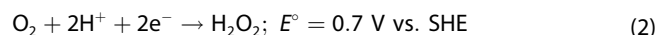
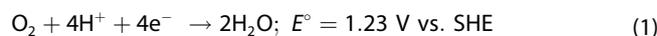


**Figure 4.** RRDE voltammetric curves in O<sub>2</sub>-saturated 0.1 M HClO<sub>4</sub> of GC disk electrodes modified with a) commercial PtNPs/C and b) Pt<sub>CF<sub>3</sub></sub> NPs/C (bottom curves). Ring electrode (top curves): Pt. E<sub>ring</sub> = 1.5 V vs. RHE, v = 10 mVs<sup>-1</sup>, 200 rpm < ω < 2000 rpm.

relatively high overpotential for both catalytic materials, especially regarding the Pt/C benchmark system. It is important to note here that we do not have put any effort to optimize our catalytic ink formulation because we have chosen to focus on the surface functionalization effect rather than striving to increase the full performance of our catalytic systems. Thus, Nafion is grossly deposited on the top of the deposited supported nanocatalysts to ensure mechanical stability of the deposits at the electrode surface (see Supporting Information) while chemical stability probed through XPS (X-ray Photoelectrons Spectroscopy) measurements is even studied with deposits free of Nafion to really evaluate possible chemical degradation of the ligands after ORR operation (see below). As a consequence, the discrepancies of the ORR efficacy observed in this work as compared to literature values may be due to this non-optimized Nafion coating since it has been shown to decrease the limiting current and to shift the potential with carbon-supported systems.<sup>[34–37]</sup>

From RRDE experiments, the number of electrons transferred per O<sub>2</sub> molecules (n) and the amount of H<sub>2</sub>O<sub>2</sub> can be monitored (Figure S6). In acidic media, O<sub>2</sub> is known to be predominantly reduced directly to H<sub>2</sub>O by a direct 4-electron pathway on platinum surfaces [Eq. (1)]. A small amount of H<sub>2</sub>O<sub>2</sub> could be produced via a 2-electron pathway [Eq. (2)] then further reduced in H<sub>2</sub>O [Eq. (3)].<sup>[38]</sup>



Almost no differences between PtNPs/C and Pt<sub>CF<sub>3</sub></sub> NPs/C are observed. For both platinum catalysts, O<sub>2</sub> is reduced through a 4-electron process with a very low produced amount of H<sub>2</sub>O<sub>2</sub> (1 to 2%), as expected. Concerning the electrocatalytic efficiency, the mass activities (MA) at 0.7 V were evaluated through the classical Koutecký-Levich analysis. MA were determined to be 174 A g<sup>-1</sup> and 202 A g<sup>-1</sup> for PtNPs/C and Pt<sub>CF<sub>3</sub></sub> NPs/C, respectively. Interestingly, this result shows that, far to have a negative impact on the ORR activity or selectivity, the covalent coating of

Pt nanoparticles even leads to a better mass activity by more than 15%.

Finally, durability experiments have been conducted to compare the stability of catalysts towards ORR, using a drastic sequence of tests coupling classical accelerated durability tests (ADT) with long-term chronoamperometry. After a scanning of the potentials between 1.10 and 0.05 V vs. RHE for 1000 cycles, a constant potential (0.7 V vs. RHE) was applied for 12 h at 900 rpm. Then LSV curves are recorded to compare the electrochemical signal before and after this durability tests sequence for both catalysts (Figure 5).

It is important to point out that a decrease of the catalytic performance is observed for both catalysts, showing, after operation, a decrease of the current density for both materials and even a shift of the onset potential toward less positive potentials for the commercial PtNPs/C (by 40 mV). It is noticeable that the catalytic activity remains still better for Pt<sub>CF<sub>3</sub></sub> NPs/C than for PtNPs/C. Interestingly, we have also measured the electrochemical surface active area (ECSA) before and after the durability test sequences. A 48% loss of ECSA can be estimated for PtNPs/C while it is limited to 24% for Pt<sub>CF<sub>3</sub></sub> NPs/C (Figure S7). The ECSA losses are generally attributed to sintering or dissolution of Pt particles. The better ECSA retention of Pt<sub>CF<sub>3</sub></sub> NPs/C compared to PtNPs/C could be explained by the molecular decoration of Pt<sub>CF<sub>3</sub></sub> NPs. The calix[4]arene coating of the Pt nanoparticles is likely to prevent such phenomena, especially thanks to the robust binding between the metallic surface and the organic moiety. However, we do observe a rather close decrease of the catalytic activity for the two catalysts despite strong differences regarding the ECSA losses (Figure 5). Consequently, the catalysts deactivation cannot be only due to possible sintering or dissolution of Pt particles in contrast to what it is generally considered. Other explanations have to be invoked such as severe corrosion of the supporting carbon material during ORR.<sup>[39,40]</sup> As suggested by Maillard et al., this corrosion leads to a loss of porosity inducing the decrease of the catalyst's ECSA, but also to a change of hydrophobicity through the formation of oxygenated surface species, responsible for the decrease of the catalytic performances. Such observations are interesting, indicating the importance of the optimization of the supporting carbon in addition to the active catalytic material itself.

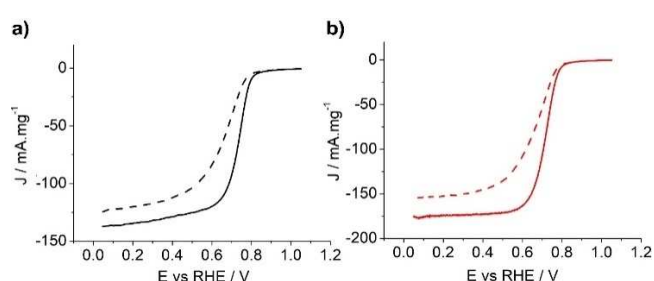


**Figure 5.** Linear sweep voltammetry (LSV) curves recorded at GC disk electrodes modified with a deposit of a) commercial PtNPs/C and b) Pt<sub>CF<sub>3</sub></sub> NPs/C before (solid lines) and after (dashed lines) durability test.  $\omega = 1600 \text{ rpm}$ .  $v = 10 \text{ mV s}^{-1}$ .

## Methanol tolerance

Having demonstrated the ORR reactivity of the chemically decorated platinum nanoparticles Pt<sub>CF<sub>3</sub></sub> NPs/C and compared with that of commercial PtNPs/C, the methanol tolerance of the two catalytic systems during ORR is now evaluated due to its importance in real applications. Methanol cross-over from the anode to the cathode results in significant performance loss at the commercial Pt/C cathode and remains a major challenge for DMFCs. Figure 6 shows the electrochemical signal for ORR before and after the addition of methanol to reach a concentration of 0.5 M. In sharp contrast to PtNPs/C, the ORR signal for Pt<sub>CF<sub>3</sub></sub> NPs/C remains slightly affected by the addition of methanol. While the same onset potential is obtained, we observe a negative shift of 80 mV of the half-wave potential and a decrease of the limiting current by 28%, but no strong signal indicating the full poisoning of the catalytic surface as for classical platinum materials. Indeed, for PtNPs/C, an anodic peak appears at 0.75 V vs. RHE. Such a peak is well-documented and is usually observed during the MOR process.<sup>[41]</sup> It corresponds to the so-called backward signal, which is assigned to the reduction/desorption processes of carbonaceous species produced upon methanol oxidation. This observation usually indicates the poisoning of the PtNPs/C catalysts. On the contrary, no peak is observed on Pt<sub>CF<sub>3</sub></sub> NPs/C, demonstrating its tolerance toward methanol.

The differences in the ORR behavior for the PtNPs/C and Pt<sub>CF<sub>3</sub></sub> NPs/C in the presence of 0.5 M methanol could be obviously attributed to the organic coating of Pt<sub>CF<sub>3</sub></sub> NPs/C. It limits the catalysts poisoning without dramatically decreasing its performances toward ORR when compared to its commercial counterpart. The reasons why the organic ligands enhance the methanol tolerance of the nanoparticles surface are not clear at this stage and beyond the scope of this paper. But steric contributions of the ligands or changes in the surface's electronic structure because of the covalent grafting may be considered. Further studies are currently in progress to better understand these results.

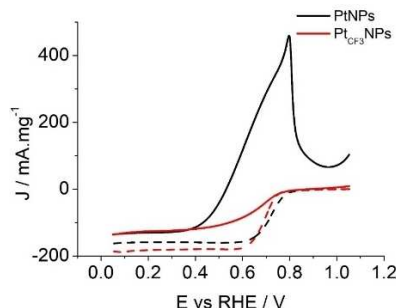


**Figure 6.** Linear sweep voltammetry (LSV) curves recorded at GC disk electrodes modified with a deposit of PtNPs/C (black) and Pt<sub>CF<sub>3</sub></sub> NPs/C (red) in O<sub>2</sub>-saturated aqueous 0.1 M HClO<sub>4</sub> containing no (dashed lines) and 0.5 M MeOH (solid lines).  $\omega = 1600 \text{ rpm}$ .  $v = 10 \text{ mV s}^{-1}$ .

MOR electrocatalytic activity of Pt<sub>CF<sub>3</sub></sub> NPs/C

The reactivity of Pt<sub>CF<sub>3</sub></sub> NPs/C for the methanol oxidation process is studied comparatively to the benchmark PtNPs/C, still under the same experimental conditions for safe comparisons. Before performing the electrocatalytic measurements, the nanocatalysts are activated by cyclic voltammetry in 0.1 M HClO<sub>4</sub> (Figure 7a).

From integration of the H<sub>UPD</sub> region, close electrochemically active surface area (ECSA) values are obtained for both catalysts (6.3 and 6.5 m<sup>2</sup> g<sub>Pt</sub><sup>-1</sup> for PtNPs/C and Pt<sub>CF<sub>3</sub></sub> NPs/C, respectively). The Pt<sub>CF<sub>3</sub></sub> NPs/C deposit also displays less capacitive current than PtNPs/C. We observed a higher current density in the 0.8–1.3 V region for Pt<sub>CF<sub>3</sub></sub> NPs/C than for PtNPs/C while the peaks associated to the Pt oxides reduction are similar for both catalysts. This suggests a more efficient formation of Pt–OH<sub>ads</sub> sites with Pt<sub>CF<sub>3</sub></sub> NPs/C than for PtNPs/C. Those sites, which correspond to the adsorption of OH groups derived from the oxidation of water, are key intermediates in the MOR process.<sup>[42]</sup> The reaction mechanisms of MOR are generally described according to two routes: an indirect pathway producing CO as intermediates towards CO<sub>2</sub> and a direct pathway forming CO<sub>2</sub>.<sup>[43]</sup> These two mechanisms are summarized in Figure 8.

Upon addition of 0.5 M methanol, the electrochemical behavior is characteristic of the MOR process for the two samples, with the observation of two peaks, one in the positive direction (*i<sub>f</sub>*) and one in the negative direction (*i<sub>b</sub>*) (Fig-

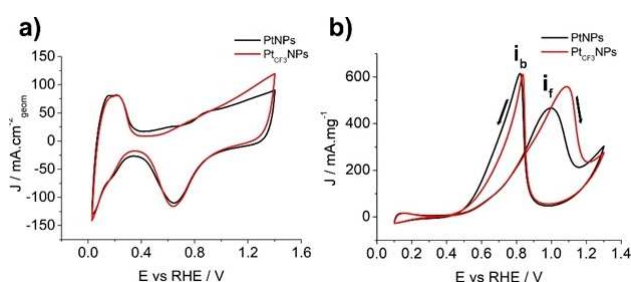


**Figure 7.** (a) Cyclic activation of NPs catalysts in 0.1 M HClO<sub>4</sub> at 10 mV s<sup>-1</sup> in the absence of MeOH; (b) CV curves at GC disks modified with deposit of PtNPs/C and Pt<sub>CF<sub>3</sub></sub> NPs/C in 0.1 M HClO<sub>4</sub> at 50 mV s<sup>-1</sup> containing 0.5 M MeOH.

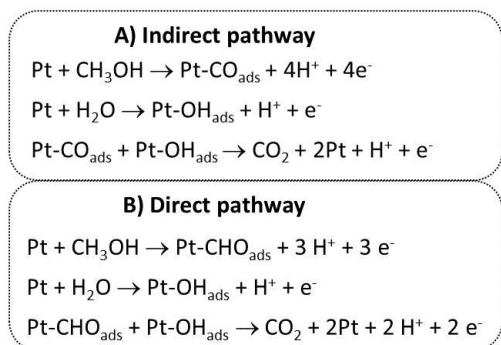


**Figure 8.** Main steps for the MOR mechanisms according to the two different pathways.

ure 7b).<sup>[5,6,43]</sup> The origins of *i<sub>b</sub>* and *i<sub>f</sub>* are still disputed,<sup>[44–47]</sup> but the *i<sub>f</sub>*/*i<sub>b</sub>* ratio is widely used as a criterion for evaluating the activity performance of the catalyst.<sup>[5,6,43,48]</sup> The larger the value, the better the activity of catalysts. Considering the curves in Figure 7b, such a criterion is obviously in favor of Pt<sub>CF<sub>3</sub></sub> NPs/C. More quantitatively, the mass activity is higher for Pt<sub>CF<sub>3</sub></sub> NPs/C (560 Ag<sup>-1</sup>) than for PtNPs/C (460 Ag<sup>-1</sup>), as well as the corresponding current density (16.8 mA cm<sup>-2</sup> and 13.8 mA cm<sup>-2</sup> for Pt<sub>CF<sub>3</sub></sub> NPs/C and PtNPs/C, respectively), suggesting that the presence of the calix[4]CF<sub>3</sub> monolayer at the platinum catalyst's surface favors the MOR activity. However, the oxidation peak (*i<sub>f</sub>*) for the Pt<sub>CF<sub>3</sub></sub> NPs/C is positively shifted with a potential equal to 1.1 V vs. RHE at maximum mass current density while this potential is 1.0 V vs. RHE for PtNPs/C. Such a behavior suggests that the methanol oxidation process is probably different with Pt<sub>CF<sub>3</sub></sub> NPs/C than with PtNPs/C, as discussed below.

As explained in the introduction, the good MOR reactivity of Pt<sub>CF<sub>3</sub></sub> NPs/C herein revealed above appears counter-intuitive with the methanol tolerance properties demonstrated by this material. It is then of importance to rationalize the observed MOR behavior. Thus, to go further in the understanding of the MOR activity of the two nanocatalysts, CO stripping experiments were performed (Figure 9 and Figure S8).

For Pt<sub>CF<sub>3</sub></sub> NPs, the CO<sub>ad</sub> potential oxidation is 80 mV more positive than that on commercial PtNPs, indicating that it is more difficult to oxidize CO at the Pt<sub>CF<sub>3</sub></sub> NPs surface. Moreover, the integration of the CO oxidation peak shows that much less CO molecules can be adsorbed onto Pt<sub>CF<sub>3</sub></sub> NPs as compared to PtNPs (a decrease by 33%). Such observations indicate that the formation of CO<sub>ads</sub> and its subsequent oxidation reaction with Pt–OH<sub>ads</sub> are obviously disadvantaged with the Pt<sub>CF<sub>3</sub></sub> NPs. They are generally considered as key steps in MOR in acidic media when mechanism A (indirect pathway) applies (Figure 8a). Because electrochemical surface areas (ECSA) determined from hydrogen desorption (H<sub>UPD</sub> region) are very similar for both catalysts, we may conclude that the grafting of the calix[4]arene layer has no significant effect on the hydrogen adsorption. In contrast, it is likely that the presence of the organic layer on the Pt<sub>CF<sub>3</sub></sub> NPs limits the adsorption of CO either because of the larger size of CO molecules compared to hydrogen and/or because of suppressing the third-body effect needed for the adsorption of CO molecules. Indeed, CO requires at least 3 adjacent Pt sites.<sup>[49]</sup> The calixarene grafting may hinder the required specific spatial

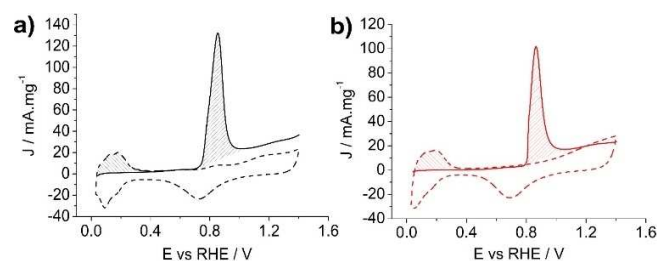


**Figure 9.** Cyclic voltammetry of a) PtNPs/C and b) Pt<sub>CF<sub>3</sub></sub> NPs/C without CO (dashed lines) and during CO stripping (solid lines) in 0.1 M HClO<sub>4</sub> at 20 mV s<sup>-1</sup>. For sake of clarity, the second scan of the CO-stripping experiments is omitted. See Figure S8 for full experimental signals.

configuration due to its geometry. Work is currently in progress by combining theoretical calculation and in situ spectroscopy to better understand this aspect. In any case, such effects lead to a behavior that agrees well with the better methanol tolerance of Pt<sub>CF<sub>3</sub></sub> NPs vs. PtNPs since the catalytic surface becomes less poisoned by CO. Now, to explain the higher MOR catalytic activity of Pt<sub>CF<sub>3</sub></sub> NPs as shown above, we need to consider that a different mechanism applies than the usual admitted one. It is generally considered that indirect pathway is the preferential mechanistic route for MOR in acidic media.<sup>[43,50–53]</sup> In the case of Pt<sub>CF<sub>3</sub></sub> NPs, a different mechanistic pathway is necessarily applied and the direct pathway is the only mechanism possible which could conciliate lower amount of the adsorbed CO and higher activity. Moreover, the direct pathway agrees well the observations above regarding the shape of Pt<sub>CF<sub>3</sub></sub> NPs voltammetry in Figure 7a. It is noticeable that a similar reasoning has been reached by Tong et al. with PVP-capped Pt nanoparticles or even with the well-performing Pt–Ru catalysts on the basis of in situ IR spectroscopic studies.<sup>[45,54]</sup> Thus, on the basis of comparison with the commercial bare platinum nanomaterial PtNPs/C, we believe that the thin layer of calix[4]arene enables us to control the operative mechanism, to some extent, and to favor the direct pathway (Figure 8b).

Eventually, the stability of the nanocatalysts is also evaluated for the MOR reaction. As for ORR, drastic sequences of stability tests were set. The potential was swept between 0.1 and 1.3 V vs. RHE for 5 cycles at 50 mV s<sup>-1</sup>, then a chronoamperometry at 0.9 V vs. RHE was recorded for 90 min. After rotation at 1600 rpm for 1 min, a new sequence cyclic voltammetry/chronoamperometry was performed for a total duration of 12 h (Figure 10).

The ECSA values are measured between each sequence. Alternation of sequences of chronoamperometries, rotation and cyclic voltammeteries enables a kind of regeneration of the catalytic surface. Indeed, a sharp decrease of current density is generally observed in chronoamperograms monitoring the methanol oxidation because of the presence of CO<sub>2</sub> bubbles and/or loosely-adsorbed intermediates at the electrochemical interface. This however does not necessarily result in the

complete deactivation of the catalyst. The current density value at the beginning of each chronoamperometry has been taken as the key parameter to compare the durability of the two catalysts. A sharper decrease of the current density is systematically observed for Pt<sub>CF<sub>3</sub></sub> NPs/C as compared to PtNPs/C (Figures 10a and b). However, the ratio of the starting current density between the first and the last chronoamperometries shows that Pt<sub>CF<sub>3</sub></sub> NPs/C exhibits a much better activity retention (94%) than PtNPs/C (71%) (Figure 10c). Such a result falls in line with the loss of ECSA in MOR which is only 7.6% for Pt<sub>CF<sub>3</sub></sub> NPs/C against 19.3% for PtNPs/C (Figure S9). In addition, it could be outlined that the current density ratio quickly drops for PtNPs/C, after the second chronoamperometry. These observations indicate that Pt<sub>CF<sub>3</sub></sub> NPs/C are much more stable and more efficient for MOR than the bare PtNPs/C. On the other hand, the sharpest decrease of the current density as observed on the different chronoamperometries for Pt<sub>CF<sub>3</sub></sub> NPs/C may be then mostly attributed to the formation of CO<sub>2</sub> bubbles, resulting from the enhancement of its MOR activity. In real DMFC devices, a catalyst reactivation during operation breaks similar to the one observed with Pt<sub>CF<sub>3</sub></sub> NPs/C would be highly desirable since it can be efficiently achieved using only a few CV cycles. Optimizing the catalyst reactivation frequency would therefore result in a prolonged lifetime and further emphasizes the appeal of using Pt<sub>CF<sub>3</sub></sub> NPs/C in a DMFC devices.

At this stage, it is important to evaluate the chemical stability of the organic coating after operation and to monitor its possible degradation since the electrocatalysis could be demanding. XPS measurements are performed with Pt<sub>CF<sub>3</sub></sub> NPs/C before and after the sequences of durability test without using Nafion top-deposit (Figure S10). These conditions are purposely chosen to evaluate the chemical stability under harsh conditions, and to mitigate a possible protective effect of the Nafion coating. It is observed that the core level spectra of Pt 4f and C 1s regions do not display significant changes. The metallic surface is not sur-oxidized and exhibits strong resistance. In addition, from the C 1s signals, specific contributions of the calixarenes moieties are extracted from the supporting carbon itself, namely the COC component at 286.3 ± 0.3 eV and the CF<sub>3</sub> component at 292.7 ± 0.3 eV. The atomic ratio COC/CF<sub>3</sub>

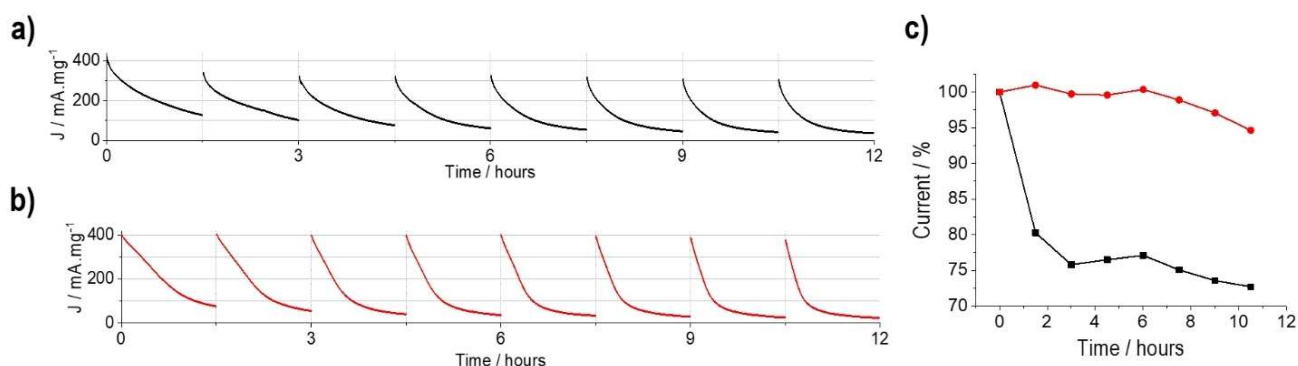


**Figure 10.** Chronoamperometry curves at 0.9 V vs. RHE for MOR reaction recorded for each sequence with deposit of a) PtNPs/C and b) Pt<sub>CF<sub>3</sub></sub> NPs/C in 0.1 M HClO<sub>4</sub> + 0.5 M MeOH. c) Variation of the current density value at the beginning of each chronoamperometry with respect to the initial current density for PtNPs/C (black line) and Pt<sub>CF<sub>3</sub></sub> NPs/C (red line).

are equal to 2.3 and 2.1 before and after the durability tests, respectively, and these values are close to the expected theoretical value of 2, indicating that the chemical footprint remains fully intact after operating the electro-oxidation of MeOH during 12 h.

## Conclusion

The functionalized calixarenes-Pt nanoparticles are demonstrated to be efficient nanohybrid catalysts exhibiting promising activity and remarkable stability for DMFC fuel cells application when compared to the commercial PtNPs/C. At first, ORR was investigated, and better performances and durability are found on Pt<sub>CF<sub>3</sub></sub>NPs with usual selectivity towards the 4-electron process. More importantly, the organic layer on Pt<sub>CF<sub>3</sub></sub>NPs/C leads to a real MeOH tolerance. In addition, a good activity along with high stability are found regarding MOR process. A facile reactivation of the catalytic materials by simply running a few CVs is evidenced. The Pt<sub>CF<sub>3</sub></sub>NPs/C are highly active MOR catalysts while being little sensitive to the presence of MeOH when operating as ORR catalysts. This intriguing and counter-intuitive behavior suggests that the MOR is likely to proceed through a more favorable direct pathway induced by the organic coating, allowing to accommodate the different experimental observations including a lower amount of Pt–CO<sub>ads</sub>, a larger amount of Pt–OH<sub>ads</sub>, a great methanol tolerance, a more difficult CO oxidation together with a high MOR activity. In situ experiments are currently in progress to confirm this assumption.

Our results demonstrate the superiority of Pt<sub>CF<sub>3</sub></sub>NPs/C for both ORR and MOR over classical Pt/C and its potential versatility in DMFCs. A single material could then be used in both anodic and cathodic compartments, without drastically hampering the performance of Pt cathodes, especially interesting for DMFC devices where the methanol crossover is unavoidable. These results highlight the potential of a molecular functionalization strategy which is easy to implement and does not require heavy set-ups and/or protocols for designing complex and shaped materials, with a risk of hampering reproducibility. It is simply based on a supramolecular concept to regulate selectivity and performances by finely tuning the interfacial properties of catalysts thanks to surface ligands.

## Experimental Section

### Chemicals

Solvents and reagents for the syntheses were at least of reagent grade quality and used without further purification. Platinum salt H<sub>2</sub>PtCl<sub>6</sub>·xH<sub>2</sub>O was purchased from Acros Organics. NaBH<sub>4</sub> and 20% PtNPs/Vulcan-XC72 powder (PtNPs/C) were purchased from Sigma-Aldrich. Calix[4]arenes-tetradiazonium salt bearing trifluorobutyl substituents (calix[4]CF<sub>3</sub>) at the small rim was synthesized using previously described procedures.<sup>[28,55]</sup>

### Synthesis of functionalized platinum nanoparticles (Pt<sub>CF<sub>3</sub></sub> NPs)

Calix[4]arene functionalized platinum nanoparticles were synthesized according to a one-pot procedure. H<sub>2</sub>PtCl<sub>6</sub>·xH<sub>2</sub>O (>99.9%, 18.2 mg, 0.0444 mmol) was dissolved in acetonitrile (25 mL). The resulting solution was then mixed with an acetonitrile solution (25 mL) containing calix[4]CF<sub>3</sub> (26.3 mg, 0.0204 mol). The mixture was vigorously stirred at 0 °C for 5 min before addition of 1 mL of a NaBH<sub>4</sub> aqueous solution (>98%, 6 mg mL<sup>-1</sup>). The color of the mixture changed from yellow to light brown after 20 min. The mixture was further stirred for 2 h at room temperature before being centrifuged at 15 000 rpm for 20 min. The bright yellow supernatant containing unreacted calix[4]CF<sub>3</sub>, Pt salts and NaBH<sub>4</sub> was removed. The left precipitate containing Pt<sub>CF<sub>3</sub></sub> NPs was washed twice by resuspension in acetonitrile followed by centrifugation until the supernatant turned to be almost transparent. The nanoparticles were finally dispersed in acetone.

*[Caution! Although no problems were encountered it is noted that diazonium salts derivatives are potentially explosive and should therefore be handled with precaution]*

The concentration of nanoparticles was determined by inductively-coupled plasma mass spectroscopy (ICP-MS) using a Thermo Scientific iCAP 7000 Series. The batch was concentrated to 450 µg mL<sup>-1</sup>.

### Transmission Electron Microscopy

High-resolution TEM (HR-TEM) was used to analyze the morphology and size distribution of the synthesized Pt<sub>CF<sub>3</sub></sub>NPs and to investigate the carbon supported Pt<sub>CF<sub>3</sub></sub>NPs/C or commercial PtNPs/C. The analyses were performed with a Jeol 2100 with an accelerated voltage of 200 V on which the images were recorded on a Gatan Orius 200 CCD camera. Size distribution was estimated with the ImageJ software, version 1.52a.<sup>[56]</sup> Lattice spacing was obtained from a FFT treatment analysis using DigitalMicrograph (Gatan).

### Scanning Electron Microscopy

In order to examine the homogeneity of the deposit, elemental mapping of the catalyst deposit onto the electrode was performed through SEM coupled with an energy-dispersive X-ray (EDX) detector, using a Jeol JSM 7100 coupled with a SDD X-Max EDX detector from Oxford instruments.

### X-ray photoelectrons spectroscopy measurements

XPS data have been collected by a Kratos Axis Nova spectrometer using the Al K $\alpha$  X-ray source working at 1486.6 eV and using a spot size of 0.7×0.3 mm<sup>2</sup>. Survey spectra (0–1000 eV) were acquired with an analyzer pass energy of 160 eV (0.5 eV/step); high resolution spectra used a pass energy of 40 eV (0.1 eV/step). Binding energies were referenced to C1s peak at 285 eV. The core level spectra were peak-fitted using the CasaXPS Software, Ltd. Version 2.3.18. U2 Tougaard or Shirley were used as background. The peaks areas were normalized by the manufacturer-supplied sensitivity factor ( $S_{C1s}=0.278$ ,  $S_{F1s}=1$ ,  $S_{O1s}=0.78$ ,  $S_{Pt4f}=5.58$ ). Concerning the durability analyses, we use deposit of Pt<sub>CF<sub>3</sub></sub>NPs/C onto screen-printed carbon electrode Dropsens since the XPS measurements cannot be made with the RRDE electrodes due to their height. The modified electrodes subsequently underwent MOR stability experiments under the same experimental conditions used for measurements with RRDE. We do not cover the deposit with Nafion in order to make the analyses simpler. For each sample, XPS

spectra were recorded on three different locations, and we did not observe any difference.

### Electrochemical analyses

A given amount of Vulcan XC-72 (Cabot Corporation) was added to the acetone suspension of Pt<sub>CF<sub>3</sub></sub> NPs to obtain a 20% Pt<sub>CF<sub>3</sub></sub> NPs/Vulcan XC-72 ink (Pt<sub>CF<sub>3</sub></sub> NPs/C), in order to compare with the commercially available 20% PtNPs/Vulcan-XC72 powder (PtNPs/C). For each sample, the volume deposited onto the glassy carbon disk electrode was adjusted to obtain a concentration of 30 μg cm<sup>-2</sup> of Pt (surface of the disk is 0.2475 cm<sup>2</sup>). After drying the ink deposit, 35 μL of an isopropanol solution with Nafion 117 (Sigma-Aldrich, 0.5%) was deposited on the surface in order to provide a better mechanical stability of the deposit at the electrode surface.

The ORR and MOR activity were evaluated using a rotating Pt/GC ring-disk electrode (37% collection rate) controlled by a Wave-Vortex 10 rotator from Pine Research. The LSV, CV and chronoamperometric scans were recorded using an Autolab PGSTAT302 N potentiostat-galvanostat (Metrohm) equipped with a BIPOT module in a conventional three-electrode electrochemical cell. A platinum grid and a SCE, KCl (sat.) electrode were used as a counter and reference electrode, respectively. Voltammograms were not corrected from iR-drop except when specified. The potentials were reported against the reversible hydrogen electrode according to  $E(\text{RHE}) = E(\text{SCE}) + 0.059 \text{ V} \cdot \text{pH} + 0.241 \text{ V}$ .

For ORR, the number of electrons ( $n$ ) exchanged can be quantified using the disk and ring currents according to Equation (4):

$$n = \frac{4I_D}{I_D + \left(\frac{I_R}{N}\right)} \quad (4)$$

where  $I_D$  is the modulus of the disk current,  $I_R$  is the ring current corresponding to the oxidation of H<sub>2</sub>O<sub>2</sub>,  $N$  is the collection rate and was determined to be 0.37 using the ferro/ferricyanide couple, in agreement with manufacturer indication.

The fraction of H<sub>2</sub>O<sub>2</sub> that is produced in the reaction can be accordingly calculated with Equation (5):

$$\% \text{H}_2\text{O}_2 = 100 \times \frac{2 \times \left(\frac{I_R}{N}\right)}{I_D + \left(\frac{I_R}{N}\right)} \quad (5)$$

The onset potential  $E_{\text{onset}}$  was determined on the LSV curves when 2% of the limiting current ( $I_l$ ) was reached.

For both ORR and MOR, the modified electrodes were activated through potential sweeping between 0.05 and 1.4 V vs. RHE at 100 mV s<sup>-1</sup> in aqueous 0.1 M HClO<sub>4</sub> until the signal was stabilized. The electrochemically active surface area (ECSA) of both series of platinum nanoparticles was measured by cyclic voltammetry at 20 mV s<sup>-1</sup> and 100 mV s<sup>-1</sup> in Ar-saturated aqueous 0.1 M HClO<sub>4</sub>. A platinum grid and a SCE electrode were used as counter and reference electrode, respectively. The ECSA value was calculated from Equation (6):

$$\text{ECSA} = \frac{H_{\text{UPD}}}{m \times C} \quad (6)$$

where  $H_{\text{UPD}}$  is the charge obtained from integration of the peak corresponding to desorption of hydrogen from the platinum surface,  $m$  is the mass of platinum as deposited and  $C$  is the monolayer adsorption charge of  $H_{\text{UPD}}$  (210 μC cm<sup>-2</sup>) that was

corrected from the supporting carbon capacity. ECSA was found to be 4.63 cm<sup>2</sup> (6.3 m<sup>2</sup> g<sub>Pt</sub><sup>-1</sup>) and 4.82 cm<sup>2</sup> (6.5 m<sup>2</sup> g<sub>Pt</sub><sup>-1</sup>) for commercial PtNPs/C and Pt<sub>CF<sub>3</sub></sub> NPs/C, respectively.

CO-stripping experiments were performed at 20 mV s<sup>-1</sup> in 0.1 M HClO<sub>4</sub> aqueous solution. First, the solution was saturated with Argon and a CV was recorded. The solution was then saturated with CO through a 30 min bubbling and a potential of 0.35 V vs. RHE was applied for 15 min. The solution was again bubbled with Argon to remove all excess of CO for 30 min. Another CV scan was then performed. The ECSA values calculated from CO<sub>UPD</sub> (420 μC cm<sup>-2</sup>) were 10.31 cm<sup>2</sup> (13.88 m<sup>2</sup> g<sup>-1</sup>) and 8.03 cm<sup>2</sup> (10.82 m<sup>2</sup> g<sup>-1</sup>) for commercial PtNPs/C and Pt<sub>CF<sub>3</sub></sub> NPs/C, respectively. These values are almost twice those found from  $H_{\text{UPD}}$  as generally reported in literature data.<sup>[57]</sup>

### Acknowledgements

This work is supported by Agence Nationale de la Recherche (ANR-21-CE50-0034-MARCEL project). Q.L. thanks the French Ministry of Research for financial support. The authors are grateful to L. Rault for the assistance in TEM experiments performed on THEMIS platform (CPER-FEDER 2007–2014) and to F. Gouttefangeas for SEM experiments performed on CMEBA platform (THEMIS/CMEBA, ScanMAT, UAR 2025 University of Rennes -CNRS, Rennes, France). B. Lefevre (ISCR- OMC, UMR 6226, University of Rennes) is thanked for his help with ICP-MS measurements. L. T.-G. is a Chercheur Qualifié of the Fonds de la Recherche Scientifique – FNRS.

### Conflict of Interest

I. J. and C. L. are shareholders of X4 C. I.J. is a consultant for X4 C. All other authors declare that they have no conflict of interest. LTG was a post-doctoral researcher for X4 C between Oct. 2014 and Sept. 2015.

### Data Availability Statement

The data that support the findings of this study are available from the corresponding author upon reasonable request.

**Keywords:** surface functionalization · electrocatalysis · diazonium grafting · methanol oxidation reaction · oxygen reduction reaction

- [1] S. S. Siwal, S. Thakur, Q. B. Zhang, V. K. Thakur, *Mater. Today Chem.* **2019**, *14*, 100182.
- [2] P. Joghee, J. N. Malik, S. Pylypenko, R. O'Hayre, *MRS Energy Sustainability* **2015**, *2*, 3.
- [3] S. K. Kamarudin, F. Achmad, W. R. W. Daud, *Int. J. Hydrogen Energy* **2009**, *34*, 6902.
- [4] N. Kakati, J. Maiti, S. H. Lee, S. H. Jee, B. Viswanathan, Y. S. Yoon, *Chem. Rev.* **2014**, *114*, 12397.
- [5] L. Yaqoob, T. Noor, N. Iqbal, *Int. J. Energy Res.* **2021**, *45*, 6550.
- [6] Y. Tong, X. Yan, J. Liang, S. X. Dou, *Small* **2021**, *17*, 1904126.
- [7] M. Sharma, N. Jung, S. J. Yoo, *Chem. Mater.* **2018**, *30*, 2.

- [8] M. Liu, Z. Zhao, X. Duan, Y. Huang, *Adv. Mater.* **2019**, *31*, 1802234.
- [9] M. Liu, X. Xiao, Q. Li, L. Luo, M. Ding, B. Zhang, Y. Li, J. Zou, B. Jiang, *J. Colloid Interface Sci.* **2022**, *607*, 791.
- [10] P. K. Babu, H. S. Kim, J. H. Chung, E. Oldfield, A. Wieckowski, *J. Phys. Chem. B* **2004**, *108*, 20228.
- [11] J. Jung, S. Kang, L. Nicolai, J. Hong, J. Minar, I. Song, W. Kyung, S. Cho, B. Kim, J. D. Denlinger, F. J. Cadete Santos Aires, E. Ehret, P. Ross, J. Shim, S. Nemsak, D. Noh, S. Han, C. Kim, B. S. Mun, *ACS Catal.* **2022**, *12*, 219.
- [12] A. K. Shukla, A. S. Arico, K. M. El-Khatib, H. Kim, P. L. Antonucci, V. Antonucci, *Appl. Surf. Sci.* **1999**, *137*, 20.
- [13] S. M. Alia, G. Zhang, D. Kisailus, D. Li, S. Gu, K. Jensen, Y. Yan, *Adv. Funct. Mater.* **2010**, *20*, 3742.
- [14] S. Sun, G. Zhang, D. Geng, Y. Chen, M. N. Banis, R. Li, M. Cai, X. Sun, *Chem. Eur. J.* **2010**, *16*, 829.
- [15] Y. Liu, Z. Li, S. Xu, Y. Xie, Y. Ye, X. Zou, S. Lin, *J. Colloid Interface Sci.* **2019**, *554*, 640.
- [16] L. Bu, S. Guo, X. Zhang, X. Shen, D. Su, G. Lu, X. Zhu, J. Yao, J. Guo, X. Huang, *Nat. Commun.* **2016**, *7*, 11850.
- [17] Y. Xu, S. Hou, Y. Liu, Y. Zhang, H. Wang, B. Zhang, *Chem. Commun.* **2012**, *48*, 2665.
- [18] J. N. Tiwari, W. G. Lee, S. Sultan, M. Yousuf, A. M. Harzandi, V. Vij, K. S. Kim, *ACS Nano* **2017**, *11*, 7729.
- [19] X. Sun, D. Li, Y. Ding, W. Zhu, S. Guo, Z. L. Wang, S. Sun, *J. Am. Chem. Soc.* **2014**, *136*, 5745.
- [20] Q. Zhao, G. Zhang, G. Xu, Y. Li, B. Liu, X. Gong, D. Zheng, J. Zhang, Q. Wang, *Appl. Surf. Sci.* **2016**, *389*, 181.
- [21] B. Ruiz-Camacho, R. Morales-Rodríguez, A. Medina Ramírez, *Int. J. Hydrogen Energy* **2016**, *41*, 23336.
- [22] Q. Lenne, A. Mattiuzzi, I. Jabin, N. Le Poul, Y. R. Leroux, C. Lagrost, *Adv. Mater. Interf.* **2020**, *7*, 2001557.
- [23] L. Lu, S. Zou, B. Fang, *ACS Catal.* **2021**, *11*, 6020.
- [24] Q. Lenne, M. Retout, B. Gosselin, G. Bruylants, I. Jabin, J. Hamon, C. Lagrost, Y. R. Leroux, *Chem. Commun.* **2022**, *58*, 3334.
- [25] D. Bélanger, J. Pinson, *Chem. Soc. Rev.* **2011**, *40*, 3995.
- [26] A. A. Mohamed, Z. Salmi, S. A. Dahoumane, A. Mekki, B. Carbonnier, M. M. Chehimi, *Adv. Colloid Interface Sci.* **2015**, *225*, 16.
- [27] A. Mattiuzzi, Q. Lenne, J. Carvalho Padilha, L. Troian-Gautier, Y. R. Leroux, I. Jabin, C. Lagrost, *Front. Chem.* **2020**, *8*.
- [28] A. Mattiuzzi, I. Jabin, C. Mangeney, C. Roux, O. Reinaud, L. Santos, J.-F. Bergamini, P. Hapiot, C. Lagrost, *Nat. Commun.* **2012**, *3*, 1130.
- [29] D. Li, Y. Luo, D. Onidas, L. He, M. Jin, F. Gazeau, J. Pinson, C. Mangeney, *Adv. Colloid Interface Sci.* **2021**, *294*, 102479.
- [30] Z.-Y. Zhou, X. Kang, Y. Song, S. Chen, *J. Phys. Chem. C* **2012**, *116*, 10592.
- [31] L. Troian-Gautier, A. Mattiuzzi, O. Reinaud, C. Lagrost, I. Jabin, *Org. Biomol. Chem.* **2020**, *18*, 3624.
- [32] Q. Lenne, A. Mattiuzzi, I. Jabin, J. Hamon, Y. R. Leroux, C. Lagrost, *Adv. Mater. Interf.* **2023**, 2202219.
- [33] K. Du, F. Ernst, M. C. Pelsozy, J. Barthel, K. Tillmann, *Acta Mater.* **2010**, *58*, 836.
- [34] S. Sharma, B. G. Pollet, *J. Power Sources* **2012**, *208*, 96.
- [35] E. Antolini, L. Giorgi, A. Pozio, E. Passalacqua, *J. Power Sources* **1999**, *77*, 136.
- [36] S. J. Lee, S. Mukerjee, J. McBreen, Y. W. Rho, Y. T. Kho, T. H. Lee, *Electrochim. Acta* **1998**, *43*, 3693.
- [37] M. Lopez-Haro, L. Guétaz, T. Printemps, A. Morin, S. Escribano, P. H. Jouneau, P. Bayle-Guillemaud, F. Chandezon, G. Gebel, *Nat. Commun.* **2014**, *5*, 5229.
- [38] A. Damjanovic, M. A. Genshaw, J. O. M. Bockris, *J. Phys. Chem.* **1966**, *70*, 3761.
- [39] L. Castanheira, L. Dubau, M. Mermoux, G. Berthomé, N. Caqué, E. Rossinot, M. Chatenet, F. Maillard, *ACS Catal.* **2014**, *4*, 2258.
- [40] L. Dubau, L. Castanheira, F. Maillard, M. Chatenet, O. Lottin, G. Maranzana, J. Dillet, A. Lamibrac, J.-C. Perrin, E. Moukheiber, A. Elkaddouri, G. De Moor, C. Bas, L. Flandin, N. Caqué, *WIREs Energy Environ.* **2014**, *3*, 540.
- [41] Y. Feng, F. Ye, H. Liu, J. Yang, *Sci. Rep.* **2015**, *5*, 16219.
- [42] M. T. M. Koper, A. P. J. Jansen, R. A. Van Santen, J. J. Lukkien, P. A. J. Hilbers, *J. Chem. Phys.* **1998**, *109*, 6051.
- [43] T. Iwasita, *Electrochim. Acta* **2002**, *47*, 3663.
- [44] A. M. Hofstead-Duffy, D.-J. Chen, S.-G. Sun, Y. J. Tong, *J. Mater. Chem.* **2012**, *22*, 5205.
- [45] D.-J. Chen, Y. J. Tong, *Angew. Chem. Int. Ed.* **2015**, *54*, 9394.
- [46] D. Y. Chung, K.-J. Lee, Y.-E. Sung, *J. Phys. Chem. C* **2016**, *120*, 9028.
- [47] P. S. Deshpande, V. R. Chaudhari, B. L. V. Prasad, *Energy Technol.* **2020**, *8*, 1900955.
- [48] R. Mancharan, J. B. Goodenough, *J. Mater. Chem.* **1992**, *2*, 875.
- [49] S. C. S. Lai, N. P. Lebedeva, T. H. M. Housmans, M. T. M. Koper, *Top. Catal.* **2007**, *46*, 320.
- [50] X. H. Xia, T. Iwasita, F. Ge, W. Vielstich, *Electrochim. Acta* **1996**, *41*, 711.
- [51] C. Lamy, A. Lima, V. LeRhun, F. Delime, C. Coutanceau, J.-M. Léger, *J. Power Sources* **2002**, *105*, 283.
- [52] T. Yajima, H. Uchida, M. Watanabe, *J. Phys. Chem. B* **2004**, *108*, 2654.
- [53] A. V. Selivanova, V. G. Demina, E. E. Aydakov, A. A. Saraev, V. V. Kaichev, V. I. Bukhtiyarov, *Appl. Surf. Sci.* **2022**, *579*, 152140.
- [54] C. Susut, D.-J. Chen, S.-G. Sun, Y. J. Tong, *Phys. Chem. Chem. Phys.* **2011**, *13*, 7467.
- [55] V. Malyskiy, L. Troian-Gautier, A. Mattiuzzi, S. Lambotte, B. Cornelio, C. Lagrost, I. Jabin, *Eur. J. Org. Chem.* **2018**, *2018*, 6590.
- [56] C. A. Schneider, W. S. Rasband, K. W. Eliceiri, *Nat. Methods* **2012**, *9*, 671.
- [57] S. Rudi, C. Cui, L. Gan, P. Strasser, *Electrocatalysis* **2014**, *5*, 408.

Manuscript received: October 27, 2022

Revised manuscript received: January 24, 2023

Accepted manuscript online: February 8, 2023

Version of record online: March 17, 2023